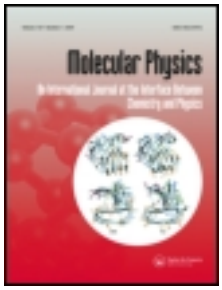

Molecular Physics: An International Journal at the Interface Between Chemistry and Physics
Publication details, including instructions for authors and subscription information:
http://www.tandfonline.com/loi/tmph20

Internal $(SiH)_X$ groups, X = 1-4, in microcrystalline hydrogenated silicon and their IR spectra on the basis of periodic DFT modelling

Alexander V. Larin [a b], Dar'ya V. Milyaeva [a], Andrey A. Rybakov [a], Dmitrii S. Bezrukov [a] & Dmitrii N. Trubnikov [a]

[a] Department of Chemistry, Moscow State University, Moscow, 119992, Russia

[b] OOO Plasmonika, Skolkovo Startup Village, Moscow Region Russia, 143025, Russia

Accepted author version posted online: 21 Jun 2013.Published online: 06 Aug 2013.

To cite this article: Molecular Physics (2013): Internal $(SiH)_X$ groups, X = 1-4, in microcrystalline hydrogenated silicon and their IR spectra on the basis of periodic DFT modelling, Molecular Physics: An International Journal at the Interface Between Chemistry and Physics, DOI: 10.1080/00268976.2013.817621

To link to this article: http://dx.doi.org/10.1080/00268976.2013.817621

Molecular Physics, 2013
http://dx.doi.org/10.1080/00268976.2013.817621

RESEARCH ARTICLE

Internal $(SiH)_X$ groups, $X = 1$–4, in microcrystalline hydrogenated silicon and their IR spectra on the basis of periodic DFT modelling

Alexander V. Larin[a,b,*], Dar'ya V. Milyaeva[a], Andrey A. Rybakov[a], Dmitrii S. Bezrukov[a] and Dmitrii N. Trubnikov[a]

[a]*Department of Chemistry, Moscow State University, Moscow 119992, Russia;* [b]*OOO Plasmonika, Skolkovo Startup Village, Moscow Region Russia 143025, Russia*

(*Received 23 April 2013; final version received 17 June 2013*)

Vibrational Si–H frequencies were calculated on the basis of density functional theory (DFT) using periodic boundary conditions for *N*-Si voids, $N < 8$, in microcrystalline hydrogenated silicon (MHS) and (100), (110), and (111) slabs of 8, 5, and 8 layers, respectively, with the dangling bonds being saturated with hydrogen atoms. The slabs are considered as the models of inter-grain boundaries (IGB) in MHS. The *N*-Si voids of different shapes have been obtained via random deleting *N* silicon atoms. It was shown that the high stretching modes (HSM) of Si–H vibrations, which are usually assigned to SiH_X, appear also due to $(SiH)_X$ groups, $X = 2$–4, in the *N*-Si voids. No such $(SiH)_X$ groups were formed with $X > 1$ at the IGB. The low stretching modes (LSM) are thus assigned to Si–H groups presented at both *N*-Si voids and IGB. Similar relative stability of the voids is obtained with two different DFT approaches, i.e., B3LYP with atomic basis set and Perdew-Burke-Ernzerhof (PBE) with plane wave basis set. This result allows a simple interpretation of usually small $I_{HSM}/(I_{LSM} + I_{HSM})$ intensity ratio as a consequence of minor concentration of any voids in device quality MHS.

Keywords: microcrystalline hydrogenated silicon; DFT; void stability; IR spectra; $(SiH)_X$ groups

Introduction

About 50% of semiconductor devices in 2010 were produced using hydrogenated silicon (HS) [1]. Despite its popularity, HS remains a puzzling metastable material whose properties in either microcrystalline hydrogenated silicon (MHS) or amorphous hydrogenated silicon (AHS) state require deeper understanding. Recent studies increased an interest to the MHS form possessing an improved ageing quality after light soaking [2,3], if special growing methods are applied. The MHS grains appear at plasma-enhanced chemistry vapour deposition of HS at high $[H_2]/[SiH_4]$ dilution together with a sharpening of the lines in X-ray diffraction spectra manifesting a quasi-phase formation [2].

The IR spectroscopy of Si–H vibrational modes is the effective instrument of HS analysis. The small value of microstructure factor (MF) expressed via ratio of respective intensities of low stretching modes (LSM) and high stretching modes (HSM) of Si–H and SiH_2 bonds, i.e., $I_{HSM}/(I_{LSM} + I_{HSM})$, is the sign of high-quality MHS for solar elements [4]. Traditionally, the LSM band (1980–2010 cm^{-1}) is assigned to Si–H bonds and to mono- or di-vacancies [5]. HSM at 2070–2100 cm^{-1} are assigned to SiH_2 groups [2,3,6–8] and to hydrogen atoms in the voids of larger radius [4,5]. The participation of the SiH_2 groups was used to explain the scissor bending frequencies around 800–900 cm^{-1} that cannot be assigned to any Si–H vibrations [6]. However, the absence of the correlation between HSM and scissor vibrations of SiH_2 around 800–900 cm^{-1} (Figure 4 in Ref. [9]) indicates the secondary role of the SiH_2 in the HSM. Alternative hypothesis about HSM assignments to the Si–H vibrations was proposed in Ref. [10] instead of the SiH_2 ones. The assignment of LSM mode to Si–H vibrations is not unique because the contributions to the LSM or HSM lines can come from Si–H groups at the inter-grain boundaries (IGB) of MHS [11]. A dependence of the LSM or HSM bands on the void size was not studied yet. The majority of the LSM and HSM assignments [2,4,5] use the Cardona model [12,13] explaining the LSM or HSM dependence on the radii *R* of the voids containing SiH_X. It predicts red shift whose absolute value increases proportionally to R^{-3} and considers the SiH_X groups as isolated.

Theoretical information about the $(SiH)_X$ distributions, $X = 1$–3, can be extracted from a direct computation of the LSM and HSM frequencies in the MHS cavities of various geometries [4,5]. Below we consider $(SiH)_X$ groups both in the voids and on the (100), (110), and (111) slabs whose surface Si atoms are saturated by hydrogen atoms. These slabs can be considered as the models of IGB in MHS. We have found that the formation of $(SiH)_X$ groups, $X = 2$–3, is the consequence of the internal tetrahedral geometry of the voids cut from bulk silicon, while no stable $(SiH)_X$ units, $X = 2 - 3$, were optimised on any of the (100), (110), and (111) slabs. The (100), (110), and (111) slab surfaces are not indeed plain (Figure S3), so one could suggest a

*Corresponding author. Email: Nasgo@yandex.ru

formation of the complex $(SiH)_X$ groups therein during the geometry optimisation. In order to check this, we manually moved closer to each other several SiH groups (relative to their regular equilibrium positions at the surface) and performed the geometry optimisation of the slab models, but we did not find any stable $(SiH)_X$ units with $X > 1$ as we observed in the voids. We used this drastic difference between the $(SiH)_X$ structures in the voids and at the IGB for the interpretation of small MF value for high-quality MHS.

Computational details

CRYSTAL06 [14] and VASP5.2.11 [15] codes were applied to the MHS models. Hybrid B3LYP (30% of Hartree–Fock exchange) [16] and PBE [17] density functional theory (DFT) functionals were used with CRYSTAL06 and VASP5.2.11, respectively. In the case of CRYSTAL calculations, we applied 88-31G*(Si)/511G*(H) basis set with the polarisation function exponents of 0.61 and 0.3 au^{-2} for Si and H, respectively [14]. Standard tolerance criteria for the treatment of the two-electron integrals of 5, 5, 5, 7, 10 (TOL1-TOL5), and DFT tolerance criteria of 9, 9, and 14 were applied. The self-consistent field (SCF) convergence parameter FMIXING, i.e., the fraction of the wavefunction converged at the previous SCF iteration, was fixed to 30%. In the case of VASP calculations, the projected-augmented wave method [15] was involved to describe the electron–ion interactions, and a plane wave basis set was employed for the valence electrons. The plane wave cut-off was set to 500 eV. Results were obtained with the PBE-generalised gradient approximation functional [18].

The supercells (SCs) of 32, 50, 54, and 64 atoms were considered as the initial models for partial Si to H replacement in the bulk. The geometry optimisation was performed using the CRYSTAL06 and VASP5.2.11 codes over 36 *k*-points in reciprocal space. The final geometry for each model was reached by the optimisation of fractional coordinates and cell parameters until all forces acting on atoms became less than 0.03 eV/Å. The (100), (110), and (111) slabs of 8-, 5-, and 8-Si layers are considered as the models of IGB in MHS. Their sides were saturated by hydrogen atoms and fully optimised. Vibrational frequencies were calculated using the finite difference method as implemented in VASP over the same *k*-grid. Small displacements (0.015 Å) of the atoms under study were used to estimate the numerical Hessian matrix. The rest of the cell atoms were kept fixed at their equilibrium positions. The clusters and periodic crystals were visualised using MOLDRAW programme [19].

Results

The stability of the MHS formation was evaluated according to the reaction scheme:

$$x\mathrm{Si} + (y/2)\mathrm{H}_2 \rightarrow x\mathrm{Si} : y\mathrm{H}, \qquad (1)$$

where Si atoms in the left part belong to crystalline phase, H_2 energy is −1.169138 au and −6.771 eV at the B3LYP/511G*(H) and PBE levels, respectively. The smaller SC of 32 atoms was modelled with both the CRYSTAL and VASP codes, while the larger SCs containing 50-, 54-, and 64-Si atoms were studied with the VASP only.

Only similar Si–H bond lengths around 1.502–1.505 Å and close frequencies of 2099.2–2074.9, 2079.1–2064.8, and 2069.8–2066.4 cm^{-1} on the (100), (110), and (111) slabs, respectively, were obtained after optimisations despite their different surface structures (Figure S3). This simple picture on the IGB without $(SiH)_X$ units, $X > 1$, is in contrast with rich vibrational structure in the MHS voids presented below.

The cell parameters of the MHS models with the voids were optimised, resulting in the densities from 2.39 (crystalline silicon) to 1.72 g/cm^3 (7-Si vacancy). The total energy per bulk Si atom used in Equation (1) is nearly constant irrespective of the SC size, i.e., PBE energy varies from −5.423 eV (total number of Si atoms $N_0 = 54$ per SC) to −5.425 eV ($N_0 = 32$, 50, and 64). The band structures for bulk silicon with conventional cell of 2-Si atoms and SC of 64 atoms were calculated (Figure S1), the first one being in agreement with Figure 2.10 in Ref. [20].

The Si to H replacement results in the formation of the $(N_0 - N)$Si:$(2N + 2)$H models, where N is the number of the deleted Si atoms. The stability per one H atom calculated with CRYSTAL and VASP according to Equation (1) versus the number of the hydrogen atoms per SC (M) is presented in Figure 1. From this figure, one can see that the most stable are 6-Si ($N_0 = 32$), 3-Si ($N_0 = 50$), 5-Si ($N_0 = 54$), and 4-Si voids ($N_0 = 64$) calculated with VASP

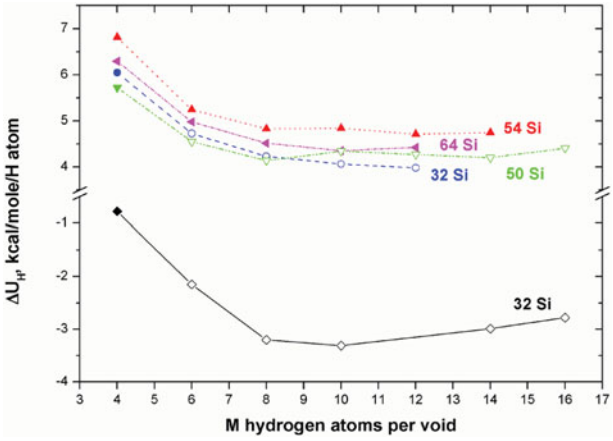

Figure 1. Energy per H atom (ΔU_H, kcal/mol/H atom) calculated with B3LYP/88-31G*(Si)/511G*(H) (diamonds) and PBE (other symbols) for super cells initially containing $N_0 = 32$ (diamonds, circles), 50 (triangles down), 54Si atoms (triangles up), and 64Si atoms (triangles left) versus the number (M) of H atoms per void. $\Delta U_H < 0$ corresponds to exothermic reaction (1). Open and closed symbols are related to isolated and connected voids, respectively.

or 4-Si vacancies for $N_0 = 32$ using CRYSTAL. For the SC of $N_0 = 32$ and 50, the 1-Si vacancies, i.e., (31Si:4H) and (49Si:4H), are isolated[1] (filled symbols in Figure 1), while the larger voids are connected forming the continued channels or pores (open symbols in Figure 1). All the voids calculated with VASP are nonstable ($\Delta U_H > 0$ in Figure 1), while the ones calculated with CRYSTAL are stable ($\Delta U_H < 0$). For the variation of the stabilities with respect to the number of H atoms (Figure 1), the isolated or connected character of the voids seems to be not important. The examples of the voids in different SCs are shown in Figures 2 and S2. By careful examination of the different models in Figure 2, one can differentiate the separate $(Si–H)_X$ groups on the basis of their close packing so that H atoms of one group are separated by 1.9–2.3 Å, which is close to 1.8 ± 0.1 Å [21] or 2.3 ± 0.1 Å [22] determined in AHS, while the shortest H. . .H distance between H atoms of the neighbour groups is larger than 3 Å. This last distance allows to decouple the Si–H vibrations of neighbouring $(Si–H)_X$ groups. In Figure 2(a), for example, we observe one separate Si–H group and three $(Si–H)_3$ ones (all of them are shown in ellipses) that fill together all 10 sites of dangling bonds obtained after removing three silicon atoms that were interconnected in the initial bulk geometry.

We will consider below for simplicity only fully occupied voids without dangling bonds in Tables 1 and 2 with the exception of 1-Si vacancy (Table 3). As demonstrated below (Table 3), increase in the concentration of dangling bonds destabilises the system. But at non-equilibrium conditions of MHS formation some of the dangling bonds remain non-saturated by hydrogen atoms; therefore, they can relax changing the void geometry. We thus consider

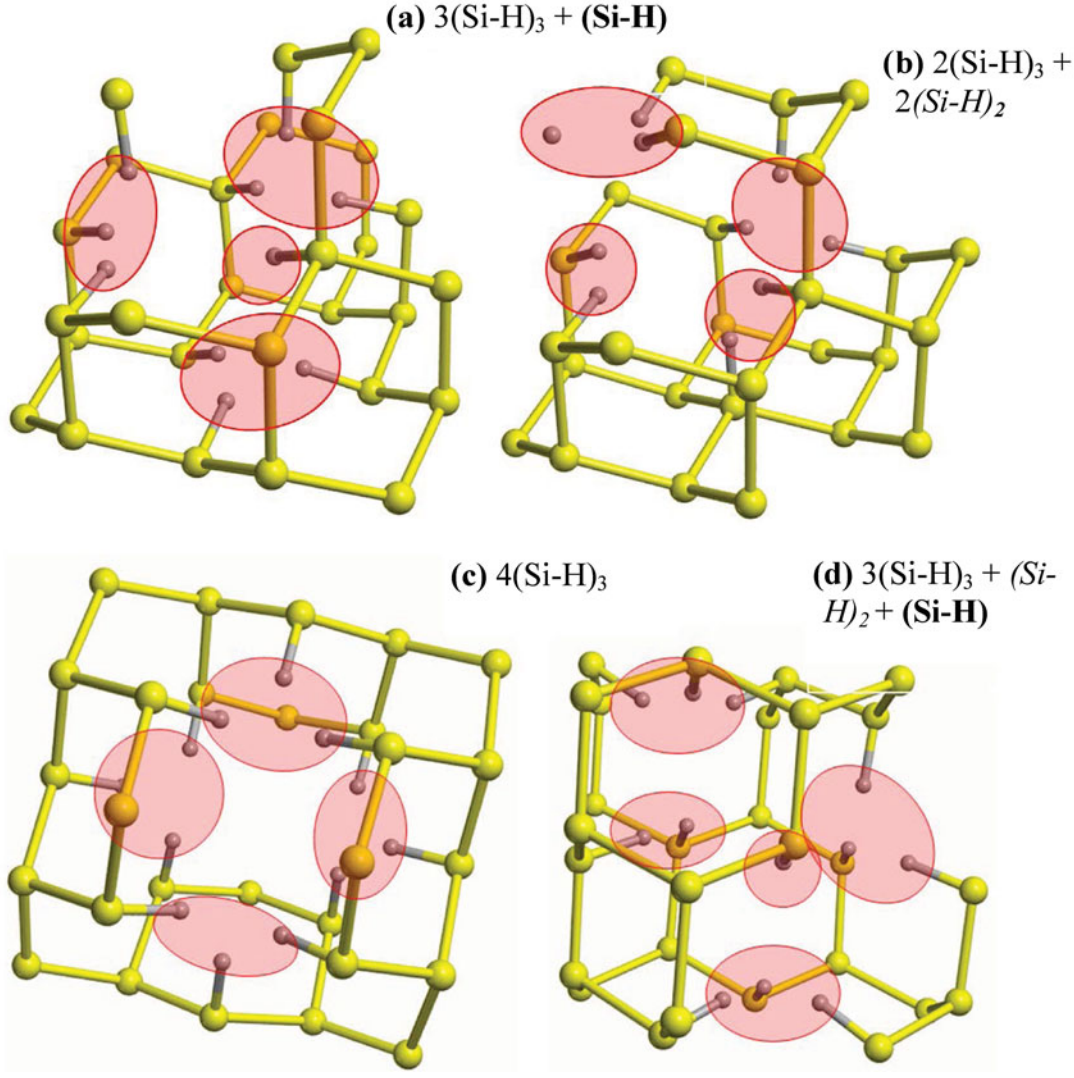

Figure 2. The geometries of the MHS voids with $N = 4$: (a) $N_0 = 50$, (b) $N_0 = 54$ and $N = 5$, (c) $N_0 = 50$, and (d) $N_0 = 54$. The colour code is as follows: Si in yellow (large spheres) and H in grey (small spheres). The separate SiH, $(SiH)_2$, and $(SiH)_3$ groups in the voids are shown by ellipses.

Table 1. The number of the $(Si–H)_X$ groups (N_X), $X = 1$–4, in the MHS voids in the SCs of $N_0 = 32$, 50, 54, and 64Si atoms (Figures 2, S2) at the PBE level (the models for $N = 1$–3 and 6 are omitted being similar for all N_0, i.e., (Si—H)$_4$ for $N = 1$, 2(Si–H)$_3$ for $N = 2$, 2(Si–H)$_3$ + (Si–H)$_2$ for $N = 3$, and 4(Si–H)$_3$ + (Si–H)$_2$ for $N = 6$). $(Si–H)_X$ for $X = 1$ and 2 are shown in bold and italic, respectively, as well as the frequencies in Table 2.

	N_0			
N	32	50	54	64
4	3(Si–H)$_3$ + (Si–H)	3(Si–H)$_3$ + (Si–H)	2(Si–H)$_3$ + 2(*Si–H*)$_2$	2(Si–H)$_3$ + 2(*Si–H*)$_2$
5	4(Si–H)$_3$	4(Si–H)$_3$	3(Si–H)$_3$ + (*Si–H*)$_2$ + **Si–H)**	3(Si–H)$_3$ + (*Si–H*)$_2$ + **Si–H)**
7	–	5(Si–H)$_3$ + **(Si–H)**[a]	–	–

[a]Respective frequency values (for 43Si:16H) are shifted to the right column of Table 2, the geometry is shown in Figure S2d.

Table 2. Frequencies (cm^{-1}) of $(Si–H)_X$ vibrations, $X = 1$–4, in the voids of MHS with $(N_0 – N)$Si:$(2N + 2)$H formulae, where N_0 is the initial number of Si atoms *per* SC with N deleted Si atoms, $N = 1$–7, at the periodic PBE level. The values for $X = 1$ and 2 are shown in bold and italic, respectively. Some void geometries are shown in Figures 2 and S2.

	N_0			
N	32	50	54	64
1	2238.5	2210.4	2237.8	2229.8
	2215.8	2180.9	2211.3	2200.2
	2209.5	2176.1	2205.6	2195.1
	2203.6	2163.5	2199.0	2191.4
2	2135.1	2157.2	2179.0	2165.9
	2126.0	2153.9	2176.8	2163.2
	2115.8	2145.4	2165.7	2156.7
	2114.7	2142.3	2162.4	2154.5
	2113.7	2138.2	2161.2	2149.2
	2105.4	2136.3	2158.4	2146.6
3	2135.1	2155.5	2178.1	2164.6
	2127.7	2147.2	2174.7	2163.7
	2126.9	2137.8	2165.0	2153.9
	2122.3	2137.0	2163.5	2152.8
	2119.4	2131.0	2156.8	2150.0
	2110.3	2126.0	2156.3	2149.2
	2095.2	*2106.3*	*2126.2*	*2116.0*
	2080.9	*2100.2*	*2111.3*	*2111.1*
4	2131.7	2149.3	2180.5	2165.6
	2130.6	2148.9	2175.9	2164.0
	2122.2	2140.9	2167.7	2152.2
	2120.6	2138.4	2164.8	2151.7
	2115.4	2134.3	2158.2	2148.2
	2114.0	2133.0	2156.6	2146.5
	2112.3	2129.2	*2130.9*	*2120.4*
	2110.5	2127.0	*2129.5*	*2114.2*
	2108.2	2121.7	*2127.5*	*2112.5*
	2060.9	**2064.1**	*2114.8*	*2104.6*
5	2120.0	2143.8	2178.1	2164.4
	2119.4	2142.3	2168.6	2161.7
	2118.4	2139.3	2165.9	2160.8
	2116.5	2133.4	2165.3	2151.8
	2112.9	2131.7	2157.9	2150.7
	2109.7	2129.7	2154.7	2150.4
	2107.4	2128.7	2153.5	2147.5
	2103.7	2126.3	2147.6	2146.9
	2101.8	2122.7	2145.6	2145.6
	2101.2	2121.8	*2125.9*	*2114.2*
	2097.3	2120.2	*2109.3*	*2111.5*
	2092.4	2116.5	**2075.5**	**2074.8**
6, 7[a]	–	2154.7	2176.8	2153.6[a]
		2150.6	2173.9	2150.0
		2145.7	2167.7	2149.1
		2138.7	2164.8	2144.3
		2138.3	2163.1	2143.1
		2137.8	2161.9	2139.9
		2137.3	2159.0	2137.9
		2133.7	2156.7	2134.2
		2126.3	2155.9	2133.2
		2125.7	2154.6	2130.0
		2123.0	2148.8	2129.1
		2117.8	2146.3	2128.0
		2110.2	**2078.1**	2123.7
		2089.4	**2070.8**	2121.1
				2118.2
				2056.9

[a]Respective 5(Si–H)$_3$ + **(Si–H)** model ($N_0 = 50$) is in the last line of Table 1.

more stable models for any SC and N-vacancy type without necessity to relax owing to the presence of the dangling bonds. As we have mentioned in Section 'Introduction', the spectra of valence Si–H vibrations are traditionally assigned to the SiH_X groups described in the literature [12,13]. One should emphasise that the partition into the $(Si–H)_X$ units inside any void used is limited by $X = 1$, 2, and 3 owing to the bulk Si geometry. It is easy to understand that X cannot be more than 4, corresponding to 1-Si. In order to differentiate between the $(Si–H)_X$ groups, the groups with the same X are denoted by the same font types in Tables 1 (geometry) and 2 (spectra), i.e., in bold and italic for Si–H and $(Si–H)_2$, respectively. For some models, the units $X = 1$ or 2 are unavoidable because of the total number of H atoms in the SC (M). For 3-Si vacancy with the $M = 8$ at least one $(Si–H)_2$

Table 3. Energies ΔU (eV), frequencies ω (cm^{-1}) of Si–H vibrations, Si–H, and H. . .H distances (Å) in 1–Si void of SC with $N_0 = 32$ and different number (1–4) of H atoms calculated at the periodic PBE level.

Model	31Si:1H	31Si:2H	31Si:3H	31Si:4H
ΔU	12.165	7.986	4.214	0.0
ω	2029.1	2119.8, 2095.4	2137.3, 2080.6, 2080.5	2238.5, 2215.8, 2209.5, 2203.6
|Si–H|	1.508	1.493, 1.499	1.494, 1.494, 1.499	1.482, 3×1.477
|H. . .H|	–	1.770	1.790, 1.802, 1.802	1.844, 2×1.857, 3×1.856

or two Si–H groups should appear if other six H atoms form two $(Si–H)_3$ units. The different combinations of the groups can be formed depending on the type of the vacancy. In this case, the 4-Si ($M = 10$) and 5-Si ($M = 12$) models are of interest. Four examples are analysed in the Figure 2 for the 4-Si (Figure 2(a) and 2(b)) and 5-Si (Figure 2(c) and (d)) types in two studied SCs. Two of the 5-Si models, i.e., for $N_0 = 32$ and 50 (Figure 2(c), coincide and thus correspond to the above-mentioned four $(Si–H)_3$ units approximately corresponding to a tetrahedral symmetry. Two other 5-Si types in the SCs with $N_0 = 54$ (Figure 2(d)) and 64 include isolated Si–H and double $(Si–H)_2$ groups denoted as $3(Si–H)_3 + (Si–H)_2 +$ **Si–H** in Table 1. This difference is only due to removing different Si atoms in the 5-Si vacancy. We would like to emphasise that this choice did not result in the appreciable energy variation between, for example, 5-Si vacancies ($M = 12$ in Figure 1) in the SCs with $N_0 = 50$ ($4(Si–H)_3$ model, Figure 2(c)) and $N_0 = 54$ ($3(Si–H)_3 + (Si–H)_2 +$ **Si–H**, Figure 2(d)). It can signify that another distribution of the $(Si–H)_X$ groups at the same N does not lead to essential energy shift probably due to slight variation of the total H. . .H repulsion.

Such geometries have simple consequences for the IR spectra.[2] Appearance of the Si–H groups is revealed in the LSM. The $(Si–H)_2$ peaks are located between the $(Si–H)_3$ and Si–H peaks, being closer to the first ones. This allows us to interpret the LSM as originated from the IGB and the isolated Si–H groups in the N-Si voids with H-filled internal surfaces, on one hand, and from the partly empty cavities (containing dangling bonds that are studied in Table 3) on the other hand. In the partly empty cavities, the concentration of Si–H and $(Si–H)_2$ groups should grow with the increase of the number of dangling bonds. However, Si–H frequencies near dangling bonds can be shifted slightly down compared to those of Si–H groups in the fully occupied N–Si vacancies, i.e., up to 2029.1 cm^{-1} (Table 3) instead of 2056.9–2078.1 cm^{-1} for Si–H groups in the voids (Table 2) or 2064.8–2099.2 cm^{-1} at IGB. This does not contradict the multi-component structure of the LSM region resolved in the MHS slabs (at 6 Torr pressure in Figure 6 in Ref. [8]). An example of the frequency variation for the $(Si–H)_X$ group in the 1-Si vacancy is given in Table 3 regarding different numbers of dangling bonds per 1-Si. It was shown experimentally [23] that the voids are essentially dehydrogenated or contain dangling bonds (after partial relaxation), so that the small concentration of the voids or small MF are accompanied by a small dangling bond concentration. SiH_2 and SiH_3 groups are also assigned to the voids [2,3,6–9], so that their HSM contributions do not contradict this conclusion. Our results are consistent with the assignment of LSM to small H clusters or isolated Si–H (2000 cm^{-1} [9]) and of HSM to large H clusters (2170 cm^{-1} [9]) by Gleason *et al*. on the basis of IR and NMR experiments [9]. The energy versus the number of dangling bonds is precisely described with linear correlation (Table 3). It allows evaluating the energy loss for the formation of one dangling bond instead of one Si–H site around 4.027 eV. This demonstrates that unfavourable dangling bond formation can happen owing to non-equilibrium conditions of the HS formation.

In order to compare the positions of calculated IR bands in the largest SC ($N_0 = 64$) with those for MHS obtained via IR spectroscopy [8], we have scaled them requiring an exact coincidence of the upper band positions, i.e., 2070 cm^{-1} from the experiment and 2210.6 cm^{-1} from the VASP computations estimated as the midrange of the $(SiH)_4$ group with the highest frequencies, i.e., $2210.6 = (2229.8 + 2191.4)/2$ cm^{-1} (Table 2). Similarly, an average frequency of 2156.9 cm^{-1} for 6 Si–H vibrations of two $(SiH)_3$ groups and an average frequency of 2113.6 cm^{-1} for two vibrations of one $(SiH)_2$ group were computed for $N = 3$ (Table 4).

Corresponding scaling factor to reach the equality of the upper peaks is thus $2070/2210.6 = 0.9364$ (double column 'MHS' in Table 4). Then frequencies of the three main groups of peaks are scaled for the three calculated $(SiH)_3$, $(SiH)_2$, and SiH series for all the models with $N_0 = 64$, yielding ∼2020, ∼1978, ∼1943 cm^{-1}, correspondingly, and three others are coming from scaled Si–H vibrations at IGB, i.e., around 1965, 1946, 1935 cm^{-1} (Table 4). Similar analogues are present for some of the peaks in experimental series, but this comparison cannot be completed without the intensity values. Taking into account a presence in the MHS voids of SiH_2 and possibly SiH_3 groups, which were not involved in our study, some absent experimental subbands (2050, 2000 cm^{-1} in Table 4) can be assigned to the bands of these groups. Hence, the absence of their computed analogues (Table 4) cannot be considered as contradicting to the $(SiH)_X$ frequency assignment. The whole width of all bands ranges for scaled and experimental series within 136.5 (Table 4) and 140 cm^{-1} [6,8], respectively. This can be considered as a good agreement.

Table 4. Calculated, scaled, and experimental [6,8] frequencies (cm^{-1}) of $(Si–H)_X$ vibrations, $X = 1–4$, in the voids of MHS or AHS with $(64 - N)Si:(2N + 2)H$ formulae, with N deleted Si atoms, $N = 1–5$, or on different (klm) Si slabs of MHS at the periodic PBE level. The values for $X = 1$ and 2 are shown in bold and italic, respectively.

			MHS		AHS	
N/(klm)	X	Calculated	Scaled[a]	Exper. [8][b]	Scaled[c]	Exper. [6]
1	4	2210.6	2070.0	2070	2140.0	2140
2	3	2156.3	2019.2	2050	2087.4	2090
3	3	2156.9	2019.8	2030	2088.0	2000
	2	*2113.6*	*1979.2*	2000	*2046.1*	
4	3	2156.1	2019.0	1980	2087.2	
	2	*2112.5*	*1977.8*	1955	*2045.0*	
5	3	2155.0	2018.0	1930	2086.2	
	2	*2112.9*	*1978.6*		*2045.4*	
	1	**2074.8**	**1942.9**		**2008.5**	
(100)	1	**2099.2**	**1965.7**		–	
	1	**2074.9**	**1943.0**		–	
(110)	1	**2079.1**	**1946.9**		–	
	1	**2064.8**	**1933.5**		–	
(111)	1	**2069.8**	**1938.2**		–	
	1	**2066.4**	**1935.0**		–	

[a]Scaling coefficient is $2070/2210.6 = 0.9364$.
[b]The experimental values are manually extracted from Figure 6 [8] with accuracy $\pm$ 3 cm^{-1}.
[c]Scaling coefficient is $2140/2210.6 = 0.9681$.

One cannot hope for an exact fit between the IR spectra computed using simple models and the complex experimental MHS data [8]. The fine structure of the Si–H valence bands are difficult to measure experimentally, that is why we have manually extracted the frequencies from Figure 6 in Ref. [8] where the conditions to reveal the details of the Si–H valence bands are realised, but no exact coordinates for each peak were presented. The Si–H valence bands were measured in the references [2–10], but the exact values were not given, while the authors crudely describe the band structure by two main HSM and LSM peaks at 2090 and 2000 cm^{-1}, respectively.

Another set of experimental peaks in AHS from Ref. [6] (right column in Table 4) is also quite close to our values calculated for N-voids. The experimental frequencies of 2140, 2090, and 2000 cm^{-1} were assigned to SiH_3, SiH_2, SiH, respectively [6]. Due to similar local geometries between AHS and MHS, we supposed that the set of the vacancies in AHS should be the same as in MHS including 1-Si model. For the demonstration of a similarity between the calculated series and the experimental frequencies in the AHS, only the frequencies in the N-Si voids were re-scaled (double column 'AHS' in Table 4) without those from the Si–H groups at the IGB, which should be only presented in MHS. After scaling the vibrational bands for all the $(SiH)_X$ groups in the vacancies from $N = 1$ to $N = 5$ (Table 4), we obtained the interval from 2140 to 2008.5 cm^{-1} nicely corresponding to the experimental AHS frequency range from 2140 to 2000 cm^{-1}. This rather confirms a similarity between the N-vacancies in AHS and MHS, and corroborates our interpretation of the results obtained for AHS and MHS. One should note that the AHS series of 2140, 2090, and 2000 cm^{-1} [6] is quite close to similar AHS data from Ref. [9], i.e., 2168, 2085, and 2029 cm^{-1}, thus providing the HSM–LSM interval of 139 cm^{-1} also nicely suiting to 140 cm^{-1} in MHS [8] (Table 4).

Conclusions

The following conclusions can be made from the above results: (1) using the DFT computations with plane waves (VASP) and atomic orbital basis sets (CRYSTAL), we have shown that the larger voids $N > 2$ are more stable than 1-Si or 2-Si; (2) vibrations in the voids correspond to spatially separated $(SiH)_X$ groups, $X = 1-4$, so that the MHS voids cannot contain the polyhydride chains in the voids because any combination of $(SiH)_X$ groups, $X = 1-3$, does not correspond to a chain; (3) the isolation of the voids does not influence their relative stabilities; (4) all the possible variants of the $(SiH)_X$ combinations in the voids of MHS are limited by the void size and shape, and by the presence of dangling bonds. The obtained results support the hypothesis [9,10] about HSM assignments to the combination of interacting Si–H vibrations of isolated $(SiH)_X$ groups. The domination of the LSM peaks in the IR band of valence Si–H vibrations in MHS of better device quality could be explained by the low concentration of all the void types whose $(SiH)_3$ groups are the source of the HSM peaks. The LSM band dominates owing to the Si–H units at inter-grain MHS boundaries. The proposed scheme of the $(SiH)_X$ locations can help to interpret a variety of possible voids in the MHS also taking into account the presence of dangling bonds and can be used for spectra modelling in an analytical mode (via Ising-like models). Taking into account the coherence between moderate sizes of the voids confirmed by NMR [9,24] or IR [9,25] experiments in device quality HS and the better stability of moderate size voids, i.e., $N = 3–4$ with CRYSTAL and $N > 2$ with VASP, the most frequently distributed voids have to be rather small. The IR contributions from Si–H vibrations in the larger N-vacancies observed in Ref. [9] can be nevertheless described via the model of $(SiH)_X$ groups presented herein.

Supplementary materials

Supplementary materials contain the figures with band structure, optimised N-Si void geometries, and the IGB models studied in the work.

Acknowledgements

The authors deeply appreciate the help of the referee to reformulate and to improve the initial version of the manuscript. A.V. Larin and A.A. Rybakov thank the financial support of Ministry of

Education and Science of Russian Federation (Minobrnauka, GK No. 07.514.11.4150). The authors thank the FUNDP, F.R.S.-FRFC (convention 2.4.617.07.F), for the use of the Namur Interuniversity Scientific Computing Facility Centre (Belgium). The authors are extremely grateful to Computer Complexes 'Lomonosov' and 'Chebyshev' of Lomonosov Moscow State University for computational time.

Notes

1. The isolated or connected character of the voids was determined visually controlling large SCs with MOLDRAW code.
2. Frequencies should be scaled to be compared to the experimental ones that can be also obtained with different values as the HSM and LSM bands.

References

[1] S. Wagner, Phys. Status Solidi A **207**, 501 (2010).
[2] V. Vavrunkova, G. van Elzakker, M. Zeman, and P. Sutta, Phys. Status Solidi A **207**, 548 (2010).
[3] M. Zeman, G. van Elzakker, F.D. Tichelaarb, and P. Sutta, Philos. Mag. **89**, 2435 (2009).
[4] W.M.M. Kessels, A.H.M. Smets, D.C. Marra, E.S. Aydil, D.C. Schram, and M.C.M. van de Sanden, Thin Solid Films **383**, 154 (2001).
[5] A.H.M. Smets, W.M.M. Kessels, and M.C.M. van de Sanden, Appl. Phys. Lett. **82**, 1547 (2003).
[6] G. Lucovsky, R.J. Nemanich, and J.C. Knights, Phys. Rev. B **19**, 2064 (1979).
[7] W.-C. Hsiao, C.-P. Liu, and Y.-L. Wang, J. Electrochem. Soc. **154**, G122 (2007).
[8] S. Ray and S. Mukhopadhyay, Phil. Magazine, **89**, 2573 (2009).
[9] K.K. Gleason, M.A. Petrich, and J.A. Reimer, Phys. Rev. B **36**, 3259 (1987).
[10] L. Lusson, A. Lusson, P. Elkaim, J. Dixmier, and D. Ballutaud, J. Appl. Phys. **81**, 3073 (1997).
[11] A. Madan and R. Martins, Philos. Mag. **89**, 2431 (2009).
[12] H. Wieder, M. Cardona, and C.R. Guarnier, Phys. Stat. Sol. A **74**, 329 (1982).
[13] M. Cardona, Phys. Stat. Sol. B **118**, 463 (1983).
[14] R. Dovesi, V.R. Saunders, C. Roetti, R. Orlando, C.M. Zicovich-Wilson, F. Pascale, B. Civalleri, K. Doll, N.M. Harrison, I.J. Bush, Ph. D'Arco, and M. Llunell, *CRYSTAL06 User's Manual* (University of Torino, Torino, 2006).
[15] (a) G. Kresse and J. Hafner, Phys. Rev. B **47**, 558 (1993); (b) G. Kresse and J. Furthmüller, Phys. Rev. B **54**, 11169 (1996).
[16] A.D. Becke, J. Chem. Phys. **98**, 5648 (1993).
[17] J.P. Perdew, K. Burke, and M. Ernzerhof, Phys. Rev. Lett. **77**, 3865 (1996).
[18] J.P. Perdew, J.A. Chevary, S.H. Vosko, K.A. Jackson, M.R. Pederson, D.J. Singh, and C. Fiolhais, Phys. Rev. B **46**, 6671 (1992).
[19] P. Ugliengo, D. Viterbo, and G. Chiari, Z. Kristall. **207**, 9 (1993).
[20] P.Y. Yu and M. Cardona, *Fundamentals of Semiconductors: Physics and Materials Properties*, 4th ed. (Springer-Verlag, Berlin, Heidelberg, 2010).
[21] D.C. Bobela, T. Su, P.C. Taylor, and G. Ganguly, J. Non-Cryst. Solids **352**, 1041 (2006).
[22] S. Chakraborty and D.A. Drabold, Phys. Rev. B **79**, 115214 (2009).
[23] A.H. Mahan, D.L. Williamson, B.P. Nelson, and R.S. Crandall, Phys. Rev. B **40**, 12024 (1989).
[24] J. Baum, K.K. Gleason, A. Pines, A.N. Garroway, and J.A. Reimer, Phys. Rev. Lett. **56**, 1377 (1986).
[25] J. Daey Ouwens and R.E.I. Schropp, Phys. Rev. B **54**, 17759 (1996).